Computer-Aided Design and Experimental Investigation of a Hydrodynamic Device: The Microwire Electrode

ARTICLE *in* ANALYTICAL CHEMISTRY · SEPTEMBER 2000

Impact Factor: 5.64 · DOI: 10.1021/ac991110v · Source: PubMed

5 AUTHORS, INCLUDING:

Fulian Qiu

45 PUBLICATIONS **848** CITATIONS

SEE PROFILE

Nicholas Stevens

The University of Manchester

44 PUBLICATIONS **442** CITATIONS

SEE PROFILE

Anal. Chem. **2000,** *72,* 3480−3485

Computer-Aided Design and Experimental Investigation of a Hydrodynamic Device: The Microwire Electrode

Qiu Fulian, Kerry A. Gooch, and Adrian C. Fisher*

Department of Chemistry, University of Bath, Claverton Down, Bath, BA2 7AY, U.K.

Nicholas P. C. Stevens

Department of Chemistry, Trent University, 1600 West Bank Drive, Peterborough, Ontario, K9J 7B8, Canada

Richard G. Compton

Physical Chemistry Laboratory, Oxford University, South Parks Road, Oxford, OX1 3QZ, U.K.

The development and application of a new electrochemical device using a computer-aided design strategy is reported. This novel design is based on the flow of electrolyte solution past a microwire electrode situated centrally within a large duct. In the design stage, finite element simulations were employed to evaluate feasible working geometries and mass transport rates. The computer-optimized designs were then exploited to construct experimental devices. Steady-state voltammetric measurements were performed for a reversible one-electron-transfer reaction to establish the experimental relationship between electrolysis current and solution velocity. The experimental results are compared to those predicted numerically, and good agreement is found. The numerical studies are also used to establish an empirical relationship between the mass transport limited current and the volume flow rate, providing a simple and quantitative alternative for workers who would prefer to exploit this device without the need to develop the numerical aspects.

The use of microelectrodes[1,4] in conjunction with hydrodynamic techniques has grown rapidly in recent years.[5−10] The motivation behind the development of such devices has been the increased versatility, the ability to monitor rapid electrochemical processes under steady-state voltammetric operating conditions, and the potential to develop new analytical devices.[1,2] To gain quantitative information using these techniques, numerical simulations have been employed to model the transport of material and chemical reactivity of the species within the electrochemical cell. Where these quantitative studies have been performed, an analytical approximation of the velocity profile within each particular cell has typically been employed.[8] As a consequence, the development of new hydrodynamic devices has been restricted to geometries and flow rates that enable analytical solutions of the velocity characteristics. More recently, we have demonstrated[11−13] that application of the finite element (FE) method to the solution of the Navier−Stokes equations allows the calculation of solution velocities for cells of arbitrary geometry, which helps to overcome the limitations noted above. In this paper, we develop our work further to address an electrode geometry that has been employed extensively in stagnant solution, the microcylinder or microwire electrode. By using our FE approach, we have been able to establish the flow characteristics of electrolyte solutions around a cylinder electrode sited within a rectangular duct (Figure 1).

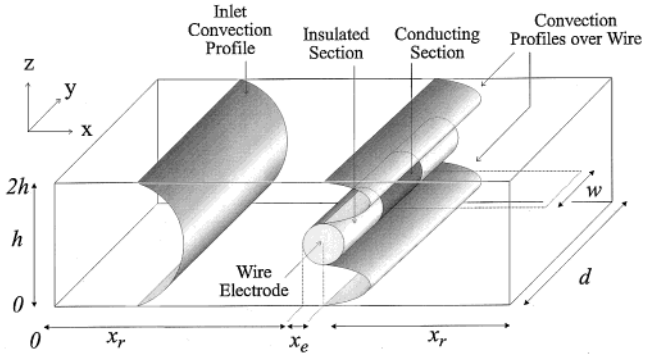

Figure 1. Schematic of the microwire cell.

(1) Wang, J. *Microelectrodes*; VCH: New York, 1990.
(2) Fleischman, M.; Pons, S. *Ultramicroelectrodes*; Datatech: Morganton, NC, 1987.
(3) Magno, F.; Lavagnini, L. *Anal. Chim. Acta* **1995**, *305*, 96.
(4) Cooper, J. B.; Bond, A. M.; Oldham, K. B. *J. Electroanal. Chem.* **1992**, *331*, 8771.
(5) Pastore, P.; Magno, F.; Lavagnini, J.; Amatore, C. *J. Electroanal. Chem.* **1991**, *301*, 1.
(6) Compton, R. G.; Fisher, A. C.; Wellington, R. G.; Dobson, P. J.; Leigh, P. A. *J. Phys. Chem.* **1993**, *97*, 10410.
(7) Compton, R. G.; Dryfe, R. A. W.; Alden, J. A.; Rees, N. V.; Dobson, P. J.; Leigh, P. A. *J. Phys. Chem.* **1994**, *98*, 1270.
(8) Aixill, A. J.; Fisher, A. C.; Fulian, Q. *J. Phys. Chem.* **1996**, *100*, 14067.
(9) Stevens, N. P. C.; Fisher, A. C. *Electroanalysis* **1998**, *10*, 16.
(10) Booth, J.; Compton, R. G.; Cooper, J. A.; Dryfe, R. A. W.; Fisher A. C.; Davies, C.; Walters, M. *J. Phys. Chem.* **1995**, *99*, 10942.
(11) Stevens, N. P. C.; Fisher, A. C. *J. Phys. Chem.* **1997**, *101*, 8259.
(12) Stevens, N. P. C.; Fisher, A. C. *J. Ann. Quim.* **1997**, *93*, 225.
(13) Fulian, Q.; Stevens, N. P. C.; Fisher, A. C. *J. Phys. Chem.* **1998**, *102*, 3779.

10.1021/ac991110v CCC: $19.00
Published on Web 06/29/2000

The simulations performed within the work presented here have two roles. First, the cell geometry and solution velocities were simulated for a range of candidate experimental cell configurations. By performing these initial simulations, it was possible to establish an experimentally sensitive configuration without the need to resort to time-consuming and expensive preliminary experiments. The second role of the simulations was in the more traditional role as an analysis tool for the experimental data recorded.

Experimental studies were performed using potassium ferrocyanide solution to evaluate the new device. Initial work focused on conditions of no solution flow, for which time-dependent analytical solutions are known.[15] Excellent agreement was observed between experimental data, analytical theory, and numerical results. Next, voltammograms were recorded for a series of volume flow rates under steady-state mass transport conditions. The results obtained are shown to fit well with those predicted numerically from the FE models.

Finally, using the numerical results, an empirical relationship between the current and volume flow rate is presented. This relationship is found to be valid for a wide range of experimentally accessible conditions and provides a simple alternative to the numerical procedures.

THEORY

In this section, we develop a model of the mass transport and electrolysis reactions occurring within the cell shown in Figure 1. The cell consists of a rectangular duct constructed of two half-cell units. A thin metal cylinder is held in the center of the cell and electrolyte solution is forced through the duct. The cylinder is insulated in the regions close to the cell walls so that only the central portion of the cylinder is employed for electrochemical measurements. In this paper, we consider the transport-limited one-electron reduction of A.

$$\mathrm{A} + e^-_{(\mathrm{m})} \rightarrow \mathrm{B}$$

When migration is neglected and the cell width, d, is significantly greater than the cell height, $2h$, the cell may be treated as being infinite in the y direction. The steady-state transport equation of interest is then given by

$$D\frac{\partial^2 C}{\partial x^2} + D\frac{\partial^2 C}{\partial z^2} - v_x\frac{\partial C}{\partial x} - v_z\frac{\partial C}{\partial z} = 0 \qquad (1)$$

where C is the concentration of the species under consideration, D is the diffusion coefficient, and v_x and v_z are the velocities in the x and z directions, respectively (Figure 1). Finite element simulations are performed to establish the velocity profile (v_x, v_z) throughout the cell by solution of the two-dimensional form of the Navier−Stokes equations, the details of which we have described previously.[11] Having calculated the velocity distribution,

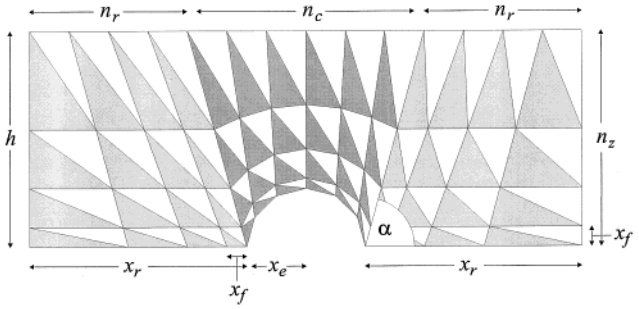

Figure 2. Grid discretization of cylinder cell.

a further finite element simulation is performed to evaluate the concentration distribution and current flowing within the cell. This procedure is performed using a grid over one-half of the cell (due to the symmetrical nature of the problem), discretised into triangular elements as shown in Figure 2.

The variables of the form $n_{\mathrm{subscript}}$ define the number of elements over the regions represented, with other variables specifying the geometry of the grid employed.

Referring to Figure 2, the following boundary conditions were employed.

x coordinate	z coordinate	boundary condition
$x = 0$	all z	$C = [\mathrm{A}]_{\mathrm{Bulk}}$
$x = 2x_r + 2x_e$	all z	$\partial C/\partial x = 0$
all x	$z = 0$	$\partial C/\partial z = 0$
all x	$z = h$	$\partial C/\partial z = 0$
electrode surface		$C = 0$

Further details regarding the numerical implementation and current calculation have been described previously.[12] All simulations were written in Fortran 90 and run on an Intel Celeron PC with 128 MB RAM. Typical CPU times varied from 300 to 600 s for the velocity distribution calculations and between 10 and 20 s for the concentration distribution simulations.

EXPERIMENTAL SECTION

A schematic of the cell is shown in Figure 1 and it can be seen to be constructed using two rectangular ducts, with the cylinder held centrally between the units. Platinum wire working electrodes (Goodfellows Metals Ltd.) of approximate radii 25 and 50 μm were employed for experimental investigations. The wires were partially coated in a nonconducting wax to leave a central region of 1−3 mm for electrochemical detection. A fully constructed cell had dimensions of height 0.095 cm, width 0.6 cm, and length 4.5 cm. The cell was held in a gravity-fed flow system, the details of which have been published previously,[6] allowing access to electrolyte volume flow rates in the region 10^{-1}−10^{-4} $\mathrm{cm}^3\ \mathrm{s}^{-1}$, where the volume flow rate is given by

$$V_{\mathrm{f}} = 4u_0hd/3 \qquad (2)$$

where d is the width of the cell in y, $2h$ is the height of the cell in z, and u_0 is the velocity at the center of the cell in z.

A silver pseudoreference electrode was sited upstream of the cell and a platinum gauze counter electrode, 80 mm × 30 mm

(14) Rius, A.; Polo, S.; Lopis, L. *Ann. Fis. Quim.* **1949**, *45B*, 1029.
(15) Aoki, K.; Honda, K.; Tokuda, K.; Matsuda, J. *J. Electroanal. Chem.* **1987**, *225*, 19.

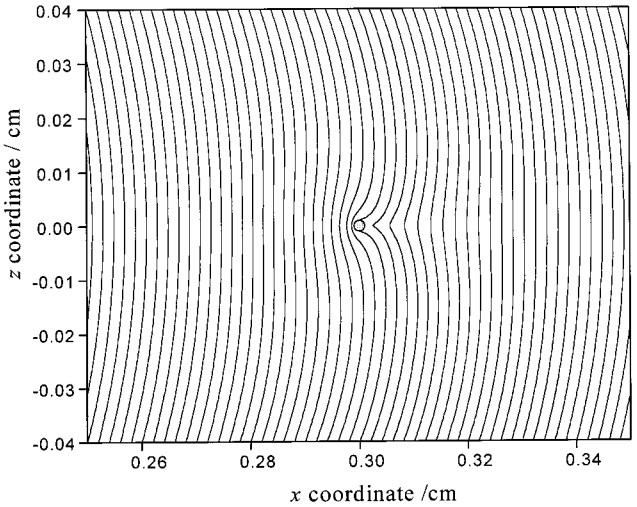

Figure 3. Flow profile above a 0.001-cm microwire electrode at center of 0.08-cm-high channel.

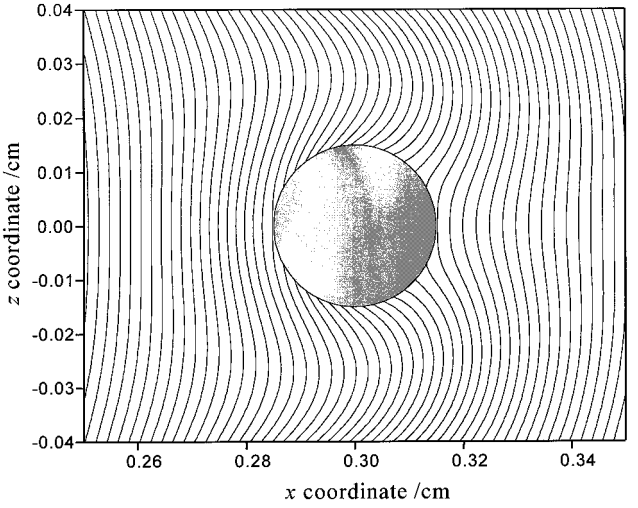

Figure 4. Flow profile over 0.025-cm microwire electrode at center of 0.08-cm high-channel.

(52 mesh), was located downstream of the working electrode. The apparatus was prepared for the experiments by flushing nitrogen-saturated solvent through the system, which acted to remove the oxygen present. Electrochemical reagents were used as supplied.

RESULTS AND DISCUSSION

Simulation. Initial simulations were performed to evaluate potential operating designs for the new cell. First, solution velocities were calculated for a range of applied pressures. A cell of dimensions similar to those used for a typical channel cell was selected: height 0.08 cm and width 0.6 cm. Simulations were performed for volume flow rates in the range 1.6×10^{-5}—1.6×10^{-2} cm^3 s^{-1} in the presence of cylindrical electrodes of sizes between 250 and 10 μm.

In the region far removed from the cylinder, a parabolic profile was established for all the flow rates considered and each calculated profile was in complete agreement with that predicted by the analytical solution.[6]

The parabolic flow profile across the whole cell is interrupted by the central electrode, and the typical flow profiles generated over two sizes of electrode, at volume flow rates of 3.2×10^{-3} cm^3 s^{-1}, are shown in Figures 3 and 4.

For the range of flow rates employed, the velocity profiles can be seen to remain broadly parabolic at any point along the cylinder surface in a manner similar to the case at the walls of the cell. No recirculation after the cylinder is observed due to the low Reynolds numbers, which result from the selected configuration and solution flow conditions.

For experimental design purposes, the conditions were chosen so that no significant circulatory behavior was observed corresponding to Reynolds numbers below 40. This was deemed desirable, as under steady-state conditions any circulatory flow would result in a region of low current density and consequently low sensitivity around the trailing edge of the electrode. It should be noted, however, that experiments performed under steady-state circulatory flow could be modeled using our approach.

Next, simulations were performed to predict the variation of the transport-limited current as a function of the solution volume flow rate. Simulations were performed using 49 different cell geometries with half-heights h of 0.02—0.08 cm and a wide range of cylindrical electrode radii between 10 and 365 μm. Centre velocities u_0 in the range 0.001—1 cm s^{-1} were used, along with diffusion coefficients between 5×10^{-6} and 2×10^{-5} cm^2 s^{-1}. The grid parameters used were $n_r = 60$, $n_c = 60$, $n_y = 60$, $x_f = 1 \times 10^{-5}$ cm, and $\alpha = 1.0$ rad, with a simulated region of 0.6 cm length, with the cylinder centrally positioned using an electrode width of 0.1 cm, and a cell width of 0.6 cm, with an electrolyte concentration of 1 mM.

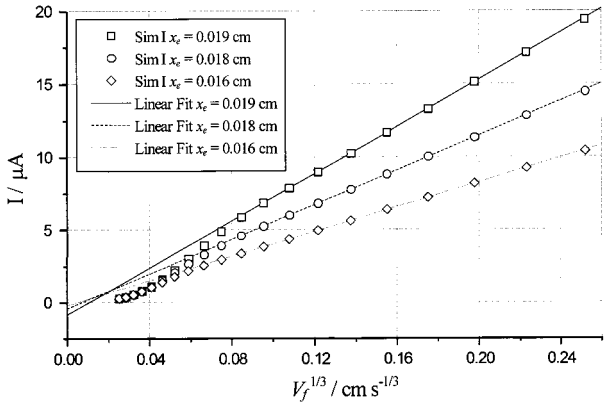

Figure 5. Current response against $V_f^{1/3}$ for three electrode radii.

Figure 5 shows the predicted current response as a function of the cube root of the volume flow rate for three electrode radii, in a cell with $h = 0.02$ cm, $[A]_{Bulk} = 1$ mM, and a diffusion coefficient of 1×10^{-5} cm^2 s^{-1}. For these examples and all other cases simulated, the current may be seen to increase linearly with the volume flow rate, above a minimum threshold, discussed in eq 6 and the following text. Note that the large values of x_e/h in Figure 5 ensure that the threshold before linearity is observed is high enough to be clearly visible at this scale.

This behavior may be rationalized by reference to Figures 6 and 7, which show the concentration profile of the reactant A close to the electrode at high- and low-volume flow rates. The general shape of the two concentration profiles is similar, with the highest current density occurring at the very front of the electrode and

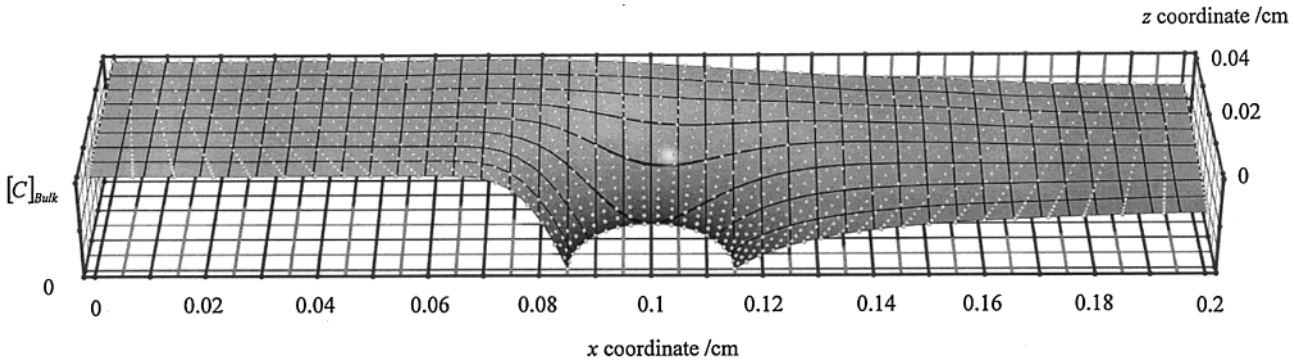

Figure 6. Concentration profile at volume flow rate 3.2×10^{-4} cm^3 s^{-1}.

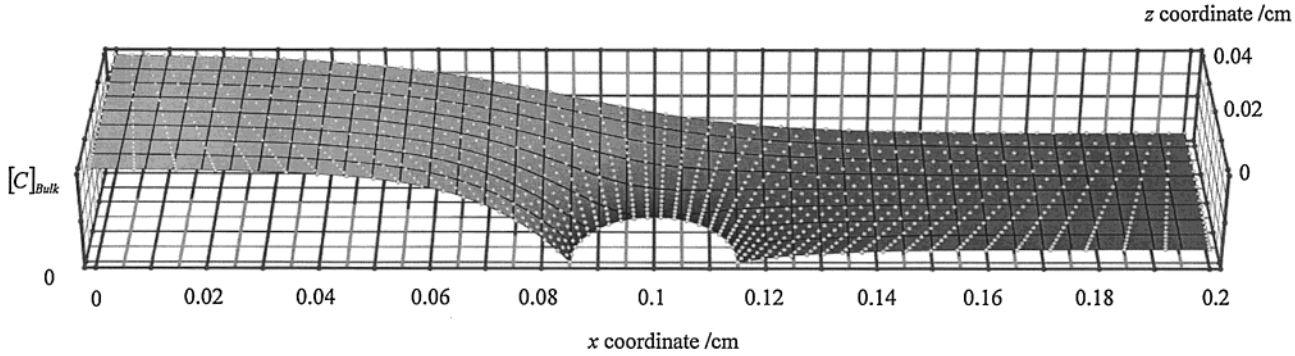

Figure 7. Concentration profile at volume flow rate 4.8×10^{-5} cm^3 s^{-1}.

the diffusion layer spreading away from the electrode as it is swept downstream. At the higher flow rate (Figure 6), the region of concentration depletion can be seen to be confined to a region closer to the electrode in comparison to the slower rate (Figure 7). Consequently, the current is significantly higher at higher flow rates, as noted in Figure 5.

Further analysis of the data collected established that for each cylinder size chosen the current response above a minimum volume flow rate was a first-order function of the cube root of the volume flow rate of the form

$$I \propto mV_f^{1/3} + c \tag{3}$$

where m and c are the gradient and intercept of the fitted lines in Figure 5. This observation can be rationalized by reference to the transport-limited current variation for the channel flow cell, which is valid for solution flowing in a parabolic and laminar manner over a flat electrode embedded into one wall of a rectangular duct and may be written as shown. The first set of parentheses encloses a dimensionless ratio, relating the size of the electrode to the height of the cell, and the second set contains the terms relating to the rates of mass transport by convection and diffusion.

$$I = 0.925\left(\frac{x_e}{h}\right)^{2/3}\left(\frac{V_f D^2}{d}\right)^{1/3} nFw[A]_{Bulk} \tag{4}$$

In many ways, the behavior observed in the microwire cell is similar, since a well-defined parabola is established when solution flows over the electrode (Figures 3 and 4), although the velocity

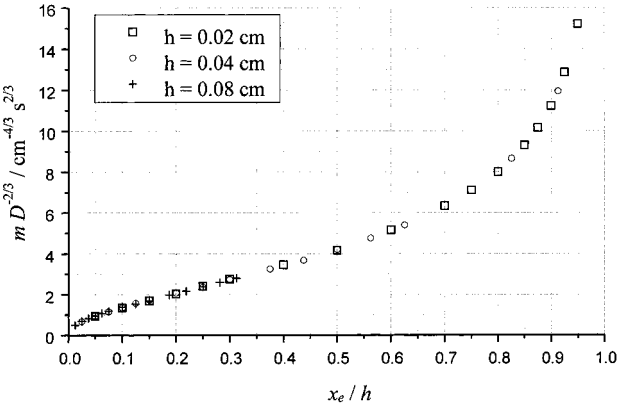

Figure 8. Variation of the parameter m.

now varies along the cell and along the electrode surface. This may explain the presence of the intercept in eq 3. We therefore examined the possibility of establishing an empirical relationship for our new geometry similar to that of the Levich equation for the channel electrode. Taking into account the intercept in eq 3, the transport-limited current for a microcylinder may be given by

$$I = (m_0(V_f D^2/d)^{1/3} + c_0 D)nFw[A]_{Bulk} \tag{5}$$

where m_0 and c_0 are functions of x_e, h, and D. It is apparent that both will be dimensionless quantities, and the results of the simulations conducted show that all plots of $m_0/D^{2/3}$ or c_0/D against the dimensionless ratio x_e/h coincide, allowing working curves to be constructed.

Figures 8 and 9 show the working curves found for m_0 and c_0, respectively, with results for three different cell heights shown.

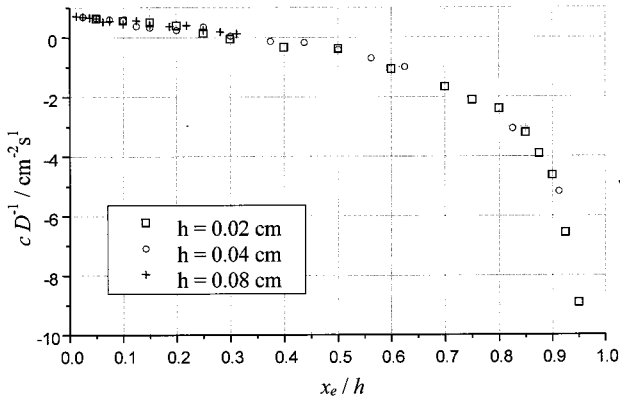

Figure 9. Variation of the parameter *c*.

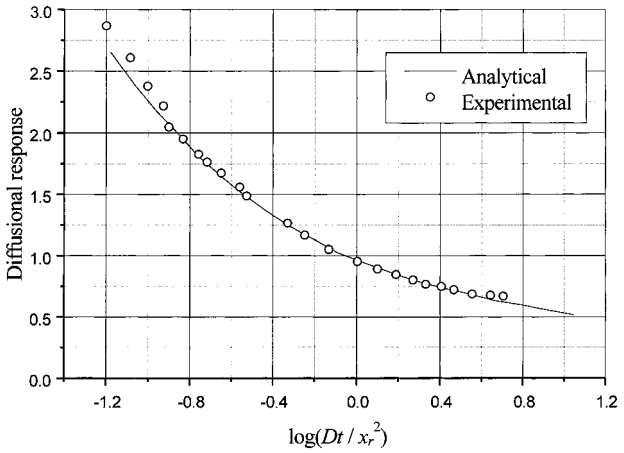

Figure 10. Response of the microwire to a potential step under no-flow conditions.

The minimum flow rate at which the current response begins to obey eq 3 may be predicted approximately by the equation

$$V_f = 10dDh/(h - x_e) \qquad (6)$$

which overestimates the minimum flow rate slightly for small ratios of x_e/h below 0.4. The nonlinearity of the current response for the cylindrical electrode below a minimum flow rate, as shown in Figure 5, is very similar to the behavior exhibited by the channel electrode. At very low flow rates, all of the material approaching the electrode is reduced leading to a current response that is proportional to V_f rather than $V_f^{1/3}$. The concentration profile shown in Figure 7 illustrates this behavior, with the diffusion layer reaching far upstream of the electrode. As the flow rate is increased, the diffusion layer shrinks in size until the bulk concentration is maintained up until very close to the electrode, as shown in Figure 6, and a linear current response is then observed with increasing $V_f^{1/3}$.

EXPERIMENTAL SECTION

First experiments were performed under conditions of no volume flow rate, since a well-known analytical relationship has been reported previously.[14,15] Figure 10 shows the results of a potential step experiment performed using a platinum wire working electrode of radius 25 μm and $w = 0.21$ cm in a buffered aqueous solution containing 1 mM potassium ferrocyanide with 0.5 M potassium chloride as the supporting electrolyte. Also shown in Figure 10 is the behavior predicted analytically and excellent agreement is noted between the two. The diffusional response function[15] is given by $Ia/2\pi nF[C]_{Bulk}D$.

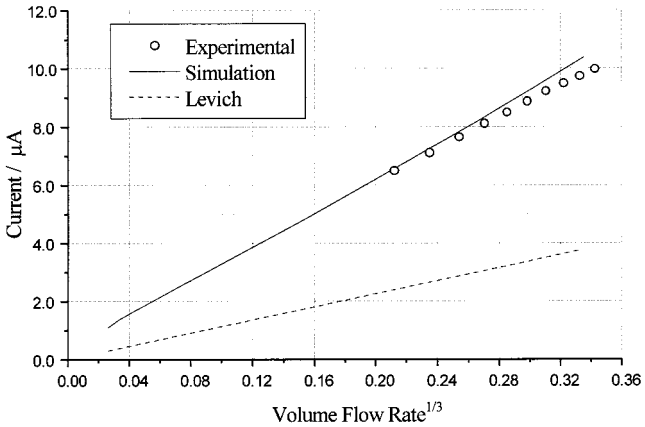

Figure 11. Steady-state response for a 12.5-μm radius wire, $w =$ 0.145 cm, and $[C]_{Bulk} = 7.1$ mM.

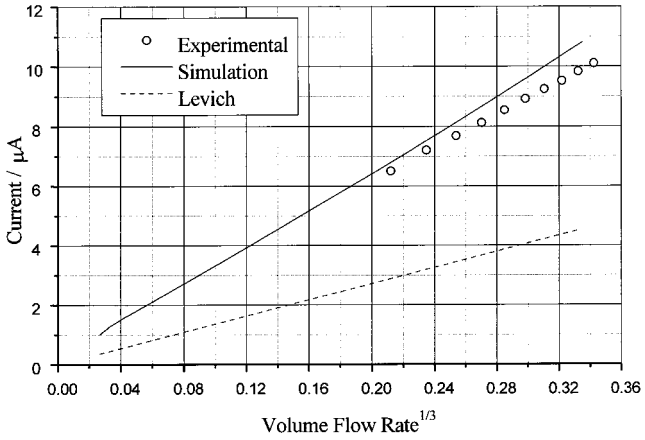

Figure 12. Steady-state response for a 25-μm radius wire, $w =$ 0.11 cm, and $[C]_{Bulk} = 7.1$ mM.

Work then focused on the hydrodynamic aspects. Voltammograms were recorded as a function of the volume flow rate using a cell of dimensions $2h = 0.94$ mm and $d = 0.60$ cm. These measurements were repeated for a range of reactant concentrations, electrode widths, and radii using 0.50 M KCl as the supporting electrolyte and the active species $K_4Fe(CN)_6$, which has a diffusion coefficient of 6.3×10^{-6} cm^2 s^{-1}. Figures 11 and 12 show two typical sets of experimental results along with the values predicted using the numerical procedures, with good agreement for both data sets. Also shown for comparison is the transport-limited current for a planar electrode of the same area as the microwire, mounted in the wall of an identical cell. The greater current density observed at the microwire due to its position at the center of the cell can be clearly noted. These results imply that, as predicted numerically, the flow profiles remain essentially noncirculatory over the range studied and that the microwire provides a useful new tool for the investigation of electrolysis processes. Work is currently ongoing to establish the transient behavior of this system and its sensitivity to mechanistic investigations.

CONCLUSION

The work presented has shown that the microwire electrode can be used under hydrodynamic operating conditions. Specifically we have been able to model the flow and diffusion characteristics within the cell as well as perform experimental investigations to establish the validity of our numerical strategy. As a result of the work presented, a semiempirical formula and working curves have been produced that establish the variation of the mass transport limited current as a function of the volume flow rate. This expression will enable workers to employ this new device without the requirement to develop the associated numerical codes.

ACKNOWLEDGMENT

We thank the EPSRC for support for N.P.C.S. and the University of Bath for support for Q.F. N.P.C.S. also thanks Professor Keith Oldham for assistance in the preparation of this paper.

Received for review September 27, 1999. Accepted April 4, 2000.

AC991110V